European Journal of Mechanics B/Fluids 29 (2010) 415–429

Contents lists available at ScienceDirect

European Journal of Mechanics B/Fluids

journal homepage: www.elsevier.com/locate/ejmflu

Considerations on shock wave/boundary layer interaction in undular hydraulic jumps in horizontal channels with a very high aspect ratio

M. Ben Meftah [a], M. Mossa [b,*], A. Pollio [a]

[a] Department of Water Engineering and Chemistry, Technical University of Bari, Via E. Orabona 4, 70125 Bari, Italy

[b] Department of Environmental Engineering and Sustainable Development, Technical University of Bari, Via E. Orabona 4, 70125 Bari, Italy

ARTICLE INFO

Article history:
Received 28 October 2009
Received in revised form
28 May 2010
Accepted 9 July 2010
Available online 19 July 2010

Keywords:
Oblique shock wave
Hydraulic jump
Turbulent boundary layer
Velocity distribution
Turbulence intensity

ABSTRACT

It can be seen in the literature that the fundamental factors governing oblique shock wave development, typically in very large channels with straight sidewalls, have not yet been completely understood and remain at the level of indicating its presence and formation. In this study, in addition to an analysis of various properties of hydraulic jump behaviour in very large channels, some aspects of boundary layer development and its detachment from the channel lateral sidewall are also investigated. At the detachment point of the lateral shock waves, it was noted that the displacement thickness experiences a significant increase; this is accompanied by a significantly reduced gradient normal to the channel sidewalls of the flow velocity as well as the occurrence of a strong, sudden adverse pressure gradient. An analysis of the flow velocity distribution and the background turbulence intensity of both the streamwise and spanwise velocity components was also carried out. Furthermore, it is argued that the supersonic flow separation analogy with a supercritical free surface flow can be applied to this case study and that the behaviour of the supercritical flow during separation can be interpreted by the free interaction theory typically used in aerodynamics.

1. Introduction

A hydraulic jump is the transition from a supercritical to a subcritical flow in an open channel. In the past the most commonly used hydraulic jump classification was that proposed by Chow [1], but it may now be considered outdated, since other authors have proposed new limits for the transitions between various types of hydraulic jumps, especially with regard to the transition between undular and classical jumps. This depends on the channel width, the Reynolds number, the boundary layer thickness development along the channel bed and the characteristics of the channel sidewall.

In the narrow region in which the transition between supercritical to subcritical flow occurs with the development of a hydraulic jump in an open channel flow, abrupt variations of flow properties are evident such as the water surface elevation and the velocity and pressure distribution, similar to those which occur for a compressible gas in the presence of a shock wave. Following this analogy, just as normal and oblique shock waves may occur for compressible gases, the same happens for hydraulic jumps, which may present wave front directions which are normal or oblique with respect to the upstream flow velocity direction.

Generally, at a certain distance from the sluice gate, lateral oblique shock waves depart from both the sidewalls with a detachment angle β (see Fig. 1, which also outlines the main geometrical quantities characterizing the jump geometry). In a wide channel, they do not cross themselves downstream of the channel because of normal shock occurrence at the channel centreline where the flow passes from a supercritical to a subcritical state. In this case, the hydraulic jump has a classical trapezoidal shape. It can be considered as typical of case I in the classification of Ohtsu et al. [2], which is different from case II where oblique shocks intersect themselves directly downstream of the detachment point if the channel is relatively narrow.

It is important to point out that there is no clear explanation for the development of lateral shock waves in an open channel with straight sidewalls. This is in contrast to the gas analogy, where shock formation is generally due to wall deflections. Many authors believe that the phenomenon is linked to lateral boundary layer development [3,2], with an abrupt increase in boundary layer thickness, its detachment from the sidewalls with a deflection angle and the generation of a recirculation region immediately downstream of the lateral shock wave [3–6].

In spite of numerous experimental studies carried out on hydraulic jumps [3,7–10,2,11,12,4–6], the fundamental factors governing shock wave development have not yet been completely

* Corresponding author. Tel.: +39 080 596 3289.
E-mail addresses: m.ben.meftah@poliba.it (M. Ben Meftah), m.mossa@poliba.it (M. Mossa), a.pollio@poliba.it (A. Pollio).

0997-7546/$ – see front matter © 2010 Elsevier Masson SAS. All rights reserved.
doi:10.1016/j.euromechflu.2010.07.002

Notations

β	Angle between the oblique shock wave and the channel sidewall or detachment angle for the shock wave (°)
γ	Specific weight (N/m^3)
θ	Inclination between the virtual solid boundary due to displacement thickness and the vertical channel sidewall (°)
θ_c	Critical value of θ in correspondence with lateral shock wave formation (°)
ν	Water kinematic viscosity (m^2 s^{-1})
ψ	Streamline function (m^2 s^{-1})
δ	Boundary layer thickness (m)
δ^*	Displacement thickness (m)
δ_c^*	Critical value of the displacement thickness in correspondence with lateral shock wave formation (m)
δ_0	Laminar sublayer (m)
ρ	Water density (kg/m^3)
τ	Wall shear stress (N/m^2)
ΔE	Energy loss per unit weight (m)
ΔE_{SW}	Additional energy loss per unit weight due to shock wave (m)
B	Channel width (m)
C_f	Total skin friction coefficient (–)
F_0	Froude number at the vena contracta (–)
F_1	Froude number at the jump toe (–)
F_{1w}	Froude number at the jump toe near the sidewall (–)
F_x	Froude number at the channel centreline at the longitudinal position x (–)
g	Gravity acceleration (m/s^2)
h_x	Flow depth at the generic longitudinal position x (m)
h_0	Flow depth at the vena contracta (m)
h_1	Flow depth at the jump toe (m)
h_{1w}, h_{2w}	Flow depth immediately upstream and downstream of the detachment point near the channel sidewall (m)
k	Critical flow depth (m)
L	Longitudinal length from the upstream channel gate to the hydraulic jump front normal to the upstream current (m)
l	Longitudinal distance from the upstream channel gate to the toe of the shock wave (m)
p	Pressure (Pa)
Q	Total flow discharge (m^3 s^{-1})
Re_x	Local Reynolds number at the longitudinal position x based on $U_1(x)$ (–)
$u = u(x, y), U = U(x, y)$	Instantaneous (u) and time-averaged (U) longitudinal velocities at the longitudinal position x and transversal position y (m s^{-1})
u', v'	Longitudinal and transversal velocity fluctuations (m s^{-1})
$U_i = U_i(x)$	Mean longitudinal free-stream velocity outside the boundary layer within the cross section at position x (m s^{-1})
U_0	Mean transversal water velocity within the cross section at the vena contracta (m s^{-1})
U_1	Mean longitudinal free-stream velocity within the cross section at the jump toe ($x = l$) (m s^{-1})
U_{1w}	Mean longitudinal water velocity upstream of the detachment point (at the jump toe) measured near the wall and immediately outside the boundary layer (m s^{-1})
$v = v(x, y), V = V(x, y)$	Instantaneous (v) and time-averaged (V) wall-normal velocities at longitudinal position x and transversal position y (m s^{-1})
x	Longitudinal coordinates from the upstream channel gate (m)
y	Perpendicular distance from the lateral sidewall (m)
y^*	Perpendicular distance from the channel sidewall (where $y = 0$) to the position of $\Psi = 0$ (m)

understood and remain at the level of indicating only its presence and formation.

Montes [13] suggested that the presence of lateral shock waves is connected with the sidewall boundary layers. He believed that the lateral boundary layer would delay the flow near the wall and force the onset of critical conditions earlier than on the channel centreline. Chanson and Montes [3] proposed that lateral shock waves were a result of the interaction of pressure distribution and lateral boundary layers. In essence, the wall boundary layer is subjected to a sudden adverse pressure gradient which causes a sharp deceleration of the flow velocity near the wall and, possibly, separation. Indeed, a recirculation of the flow indicating separation can be observed immediately behind the lateral shock waves near the wall.

Reinauer and Hager [14] argued that the supercritical free surface flows are prone to shock waves. Surface waves originate from various types of disturbances such as the deflection of the lateral sidewall direction, the presence of a disturbance from the channel bottom geometry and discharge and boundary roughness variations along the channel.

Because of their intrinsic importance, the strong viscous interactions between boundary layers and shock waves have been extensively studied over the past 50 years for industrial and aerodynamic purposes and are still the subject of active research due to their complexity and the difficulty of predicting them, especially in a turbulent regime [15].

The majority of these studies have concentrated on shock wave/boundary layer interaction, where the shock waves were generated at given positions and under specific conditions such as wall deflection. However, it was observed that there is a lack of data concerning the conditions of the incoming boundary layer when the lateral shock wave takes place in a large rectangular channel with a constant discharge and roughness of its bottom and lateral walls and without any modification of its section or wall inclination.

The principal focus of this study is to describe some features of investigated hydraulic jumps in terms of the boundary layer development at the sidewall. This process results in lateral boundary layer separation due to the presence of an adverse pressure region downstream of the lateral shock wave front.

2. Theoretical background

When water enters a channel, the velocity distribution across the channel section will vary with the distance over which the water travels owing to the presence of a boundary layer [1]. The fluid particles at the surface of the laterally bounding channel walls have zero velocity and they reduce the velocity of adjacent particles in the transversal direction; this also occurs at the channel bottom. Therefore, for a prismatic channel of constant wall roughness, the lateral boundary layer can be presented as shown in Fig. 2. The boundary layer thickness is denoted by δ and has been defined as the normal distance from the boundary surface (lateral channel wall) at which the longitudinal component of the water velocity U is equal to 0.99 of the limiting velocity U_i (depending

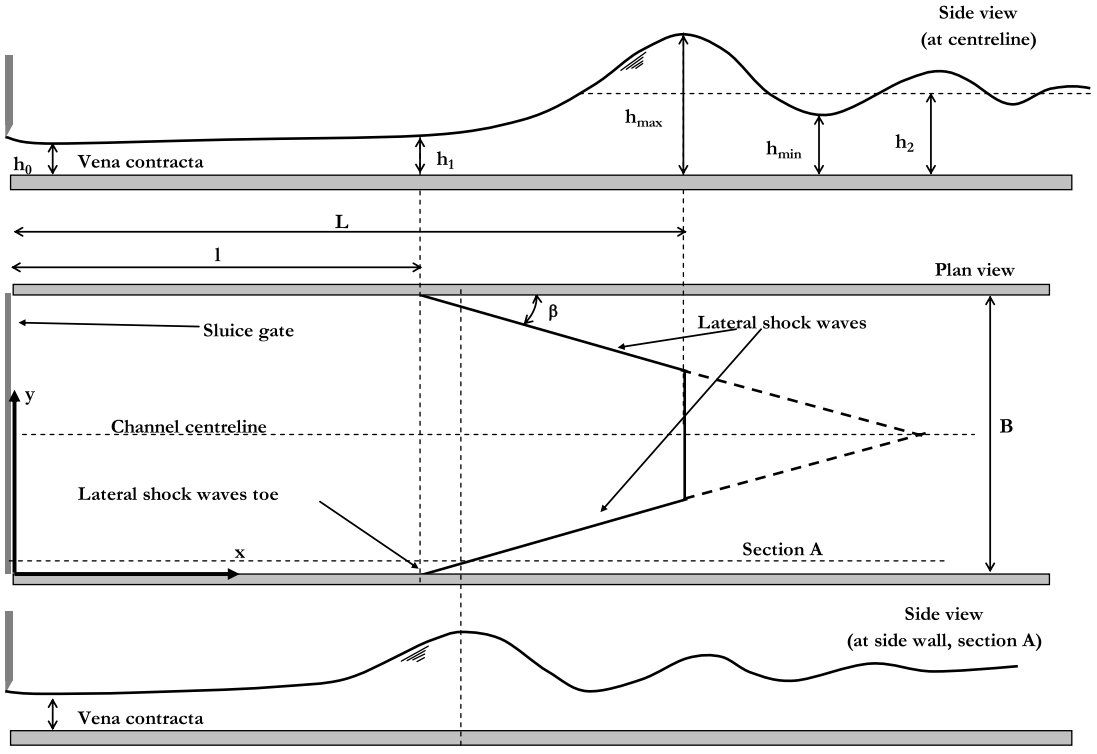

Fig. 1. Sketch of a typical undular jump geometric configuration in a very large channel.

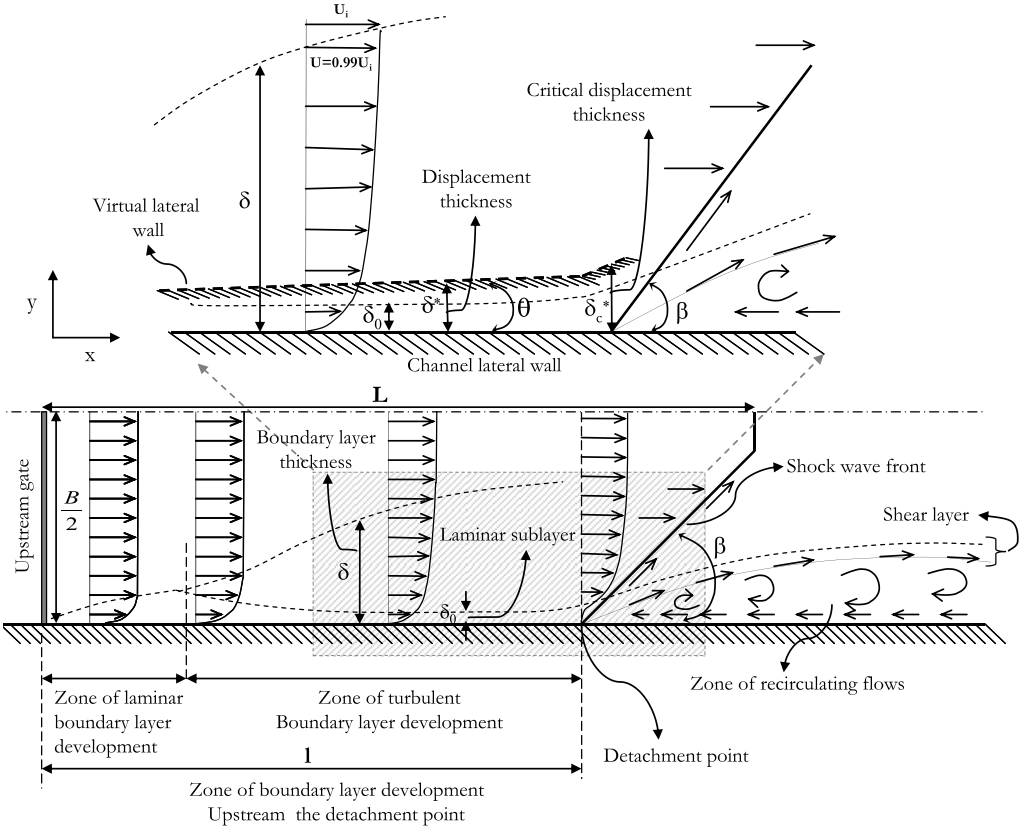

Fig. 2. Definition sketch of the development of the boundary layer at the lateral channel wall with the presence of a shock wave front.

on longitudinal position x) which is the free-stream water velocity outside the boundary layer (zoomed area of Fig. 2). According to literature [1] the effect of the boundary layer on the flow is equivalent to a fictitious displacement of the surface boundary to

a virtual position (see enlarged area of Fig. 2) by an amount equal to the so-called displacement thickness δ^*, which is defined as

$$\delta^* = \int_0^{\delta} \left(1 - \frac{U}{U_i}\right) dy \tag{1}$$

where U is the time-averaged longitudinal component of the water velocity at the generic distance y from the channel wall. If the free-stream velocity U_i is not constant along the channel axis direction, δ^* is variable with the longitudinal distance x from the channel inlet.

Generally, the value of the displacement thickness varies from one-eighth to one-tenth of the boundary layer thickness δ, depending on the magnitude of the Reynolds number [1]. By using experimental data, Eq. (1) may be approximated by considering discrete Δy intervals, with the following equation

$$\delta^* = \sum \left(1 - \frac{U}{U_i}\right) \Delta y. \tag{2}$$

Several other methods have been proposed to calculate the displacement thickness of the turbulent boundary layer for two-dimensional flows along flat surfaces. An approximate but practical method [16] was adopted to estimate δ^* on the channel sidewalls using

$$\delta^* = \frac{\delta}{8} = 0.162\, \mathrm{Re}_x^{-1/7} \frac{x}{8} \tag{3}$$

where

$$\mathrm{Re}_x = \frac{U_i x}{\nu} \tag{4}$$

is the local Reynolds number at the longitudinal position x from the channel upstream gate and ν is the water kinematic viscosity.

Since the boundary layer thickness increases with the distance x from the vena contracta (which is close to the upstream gate), and since the displacement thickness is proportional to the boundary layer thickness, the virtual lateral wall caused by the displacement thickness can be presented as a vertical, almost-flat plate of angle θ with respect to the lateral channel wall, as shown in Fig. 2. At a certain distance l from the upstream gate, the displacement thickness undergoes a sharp increase and reaches a critical value, δ_c^*, leading to an immediate increase of angle θ to a critical value θ_c. At this position, the flow depth h in the channel increases strongly which results in an increase of the potential flow energy, leading to a reduction in the kinetic energy and a deceleration of the fluid flow. When this happens, an adverse pressure gradient occurs in the boundary layer and at some distance from the wall, the longitudinal velocity gradient becomes nil ($\partial U/\partial y = 0$), and thus the wall shear stress τ_w becomes negligible. This strong, sudden adverse pressure gradient generates a separation of the boundary layer and a detachment of the lateral shock wave takes place.

In several early experimental investigations of supersonic flows (see for example, [17]), the separation of a boundary layer is the result of an upstream propagation of a compressive disturbance which induces a rise in pressure along the wall surface. A theoretical explanation for the propagation of the disturbance upstream was given by Lighthill [18] in the context of a linear theory which is valid for disturbances of a small amplitude. He argued that a compressive disturbance gives rise to an adverse mainstream pressure gradient, and once the disturbance is of sufficient strength, boundary layer separation must occur. As a consequence, a relatively large boundary layer thickness can act to alter the external flow by provoking a pressure rise ahead of the separation point (detachment point), which in turn causes the flow to separate upstream of it. This phenomenon is often called self-induced separation [19].

Using the analogy of supersonic flow separation (see also [20,21] for further details), the behaviour of the supercritical flow in our tests during the separation can be interpreted by the free interaction theory, even though some aspects of the phenomenon do not fit with this simple theory, particularly for turbulent interaction [15]. This theory establishes that the flow depth rise from h_{1w} to h_{2w} during the separation of a supercritical boundary layer is described by the following relationship

$$\frac{g\left(h_{2w}^2 - h_{1w}^2\right)}{h_{1w} U_{1w}^2} \propto \left(C_f\right)^{-\frac{1}{2}} \left(F_{1w}^2 - 1\right)^{-\frac{1}{4}} \tag{5}$$

where h_{1w} and h_{2w} are the flow depths just upstream and downstream of the detachment point (toe of the jump) close to the channel sidewall, U_{1w} and F_{1w} are the time-average longitudinal velocity and the Froude number corresponding to h_{1w}, and C_f is the total skin friction coefficient. The coefficient C_f can be calculated with the following equation

$$C_f = \frac{0.074}{\mathrm{Re}_x^{0.2}} \quad \text{for } 5 \cdot 10^5 \le \mathrm{Re}_x \le 10^7 \tag{6}$$

as shown by Schlichting [16], supposing the validity of the 1/7-th-power law for velocity distribution and a turbulent boundary layer from the sluice gate position. In a different way, assuming the logarithmic velocity distribution law, the skin friction coefficient can be calculated by the empirical relationship proposed by Schlichting [16]

$$C_f = \frac{0.455}{\left(\mathrm{Log}\, \mathrm{Re}_x\right)^{2.58}}. \tag{7}$$

Eqs. (6) and (7) are a result of the assumption that the velocity profiles in the boundary layer on a plate and into a pipe are identical. On the basis of measurements on a flat plate, Shultz-Grunow [22] proposed the following equation

$$C_f = 0.427\, (\mathrm{Log}\, \mathrm{Re}_x - 0.427)^{-2.64} \quad \text{for } \mathrm{Re}_x \ge 10^6. \tag{8}$$

Nikuradse [23], after a series of experiments on a flat plate, suggested

$$C_f = 0.02666\, \mathrm{Re}_x^{-0.139} \quad \text{for } \mathrm{Re}_x \ge 10^6. \tag{9}$$

3. Description of experimental tests

The experiments were carried out at the Technical University of Bari, Italy, at the Coastal Engineering Laboratory (L.I.C.) of the Water Engineering and Chemistry Department. The experimental apparatus consisted of a rectangular steel channel with a surface base of 15 m by 4 m and a channel depth of 0.4 m. Since the water depth was particularly shallow for all tests, a 2D Nortek ADV system was used in order to measure the longitudinal and transversal components of the water velocity along directions x and y, respectively, at a distance of 1 cm from the channel bottom. The 2D ADV was used with a sampling rate of 25 Hz, a sampling volume of less than 0.25 cm^3, a velocity resolution of 0.1 mm/s and a random noise of approximately 1% of the velocity range at 25 Hz. Furthermore, the water height was measured using an ultrasonic measuring system. For further details on the description of the experimental set-up, see [4–6]. Since the channel walls are made of transparent glass, a relatively smooth material, the effects of wall roughness on the boundary layer are not considered in this study.

In the present study, the analyzed hydraulic jumps took place in a very large channel. All the tests were characterized by an aspect ratio of $B/k = 100$, where B is the channel width and $k = (Q^2/(gB^2))^{1/3}$ is the flow critical depth.

Chanson and Montes [3] presented a table where they reported the lower and upper limits for various jump types. In particular, for types D and E the ranges of the inflow Froude numbers are 1.35–2.40 and 2.40–2.91, respectively. In their work, the authors considered flows characterized by the aspect ratio $B/k = 2.20$–13.33. Following the classification of Chanson and

Table 1
Main quantity values for the tests.

Test	Jump type [3]	F_0 (-)	h_1 (cm)	U_1 (m/s)	F_1 (-)	Re_1 (-)	β (°)	l (m)	L (m)
T1	D	3.06	2.74	0.91	1.76	7.64E+05	63	1.1	1.7
T2	D	3.51	3.31	0.76	1.33	1.20E+06	47	1.5	2.8
T3	E	3.72	1.94	1.29	2.96	2.02E+06	58	1.5	2.0
T4	D	3.89	1.81	1.38	3.27	2.57E+06	41	1.7	3.6
T5	D	3.90	2.37	1.05	2.18	1.29E+06	47	1.6	3.1
T6	D	4.80	2.31	1.08	2.27	1.73E+06	44	2.1	3.9
T7	D	6.40	2.42	1.03	2.11	2.06E+06	37	2.7	5.1
T8	D	8.28	2.53	0.99	1.99	3.35E+06	40	4.6	6.1

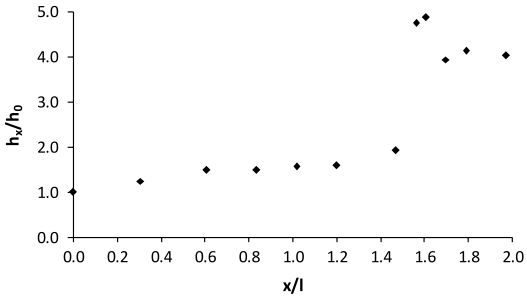

Fig. 3. Dimensionless tailwater along the longitudinal channel centreline (test T1, $F_0 = 3.06$).

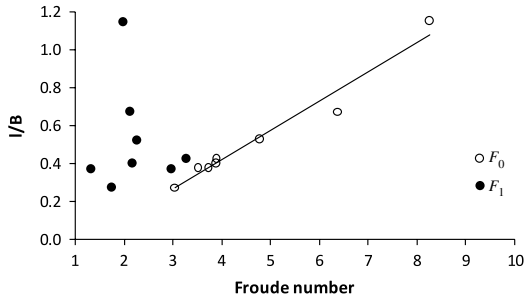

Fig. 4. Relationship between the Froude numbers F_0–F_1 and the ratio between the distance l of the detachment point from the sluice gate and the channel width B (the continuous black line is Eq. (10)).

Montes [3], the hydraulic jumps analyzed in the present study can be classified as type D, except for test T3 which is type E, with the development of rollers at the first wave crest and bubble air entrainment in the same zone. Table 1 reports the main quantities for all the tests carried out, which are described below. The water discharge $Q = 0.100$ m^3/s was constant over all tests. The mean water height h_1 within the cross section at the toe of the jump, immediately upstream of the detachment of the lateral shock wave (when $x = l$) was obtained from direct measurements. In the same cross section, the mean transversal water velocity U_1 was calculated from Q and h_1, and the Froude number at the toe of the jump F_1 was evaluated as $U_1/(gh_1)^{0.5}$. F_0 is the inflow Froude number at the vena contracta and is always higher than F_1. Table 1 also shows the local Reynolds number $Re_1 = U_1 l/\nu$, the detachment angle β and the distances l and L between the sluice gate and the detachment point and the first crest wave, respectively (see also Fig. 1). It must be highlighted that, in each test, the mean free-stream longitudinal velocity U_i, at the supercritical flow region, varies along the centreline with x because the tailwater increases slightly from the vena contracta, immediately downstream of the sluice gate, to the jump toe, as shown in Fig. 3.

In order to obtain more information on turbulent flow structures, accurate measurements of the flow velocity were taken for various tests (T3,T4 and T8) at several points along only one-half of the channel horizontal plane, as a result of flow symmetry with respect to the channel longitudinal centreline.

4. Results and discussion

4.1. Froude number effect on the position of the separation of the boundary layer and on the detachment angle value

The inflow Froude number F_0 greatly affects the longitudinal position of the jump front [10], as can be seen in Fig. 4, which shows the distance l of the jump toe from the sluice gate dimensionlessed by the channel width B as a function of F_0. The linear trend curve in the figure gives the following equation

$$\frac{l}{B} = 0.15\,(F_0 - 1.33)\,, \qquad R^2 = 0.96 \tag{10}$$

where R^2 is the square of the correlation coefficient.

Clearly, the higher the inflow Froude number F_0, the more distant the longitudinal position l at which the lateral shock waves (jump toe) occur. Thus, we can clearly see the significant and proportional effects of the inflow Froude number F_0 on the position of the detachment point for the oblique front of the jumps. This implies that F_0 affects the flow characteristics [whether it is fully developed or not [10]] and determines how far away from the sluice gate the jumps form. On the other hand, the Froude number F_1 at the jump toe affects the specific features of the jumps [or rather their type, see also the works in the bibliography, for example [3]]. Moreover, from Fig. 5 it can be noted that the detachment angle β clearly decreases with the increase of F_0 in the same way as in the theoretical equation proposed by Ippen [24]

$$\sin\beta = \frac{1}{F_0}\sqrt{0.5\,\frac{h_2}{h_0}\left(1 + \frac{h_2}{h_0}\right)} \tag{11}$$

so confirming the classical theory of shock waves in supercritical flows, even if in our case the detachment angles exceeded those obtained by Eq. (11). This may be explained by observing that the supercritical flow speed is not constant along the longitudinal channel axis, as Ippen [24] theorized, but indeed was reduces in our tests, consequently affecting detachment angle values.

In the present study, the experimental detachment angles can be fitted by the following power law as a function of F_0.

$$\beta\,(F_0) = \frac{85.33}{F_0^{0.41}}. \tag{12}$$

Furthermore, it is worthwhile observing that if the detachment angles are plotted as a function of the Froude number F_1 (measured at the jump toe as shown in Fig. 6), the conclusions of Chanson [25] and Ohtsu et al. [2], reported in Eqs. (13) and (14) respectively, seem to be more suitable to describe the phenomenon compared to those of Eq. (15) determined by Engelund and Munch-Petersen [26].

$$\beta = 28.1\,F_1^{0.38} \tag{13}$$

$$\beta = 32\,F_1^{0.57} \tag{14}$$

$$\beta = 57.3\,F_1^{-1}. \tag{15}$$

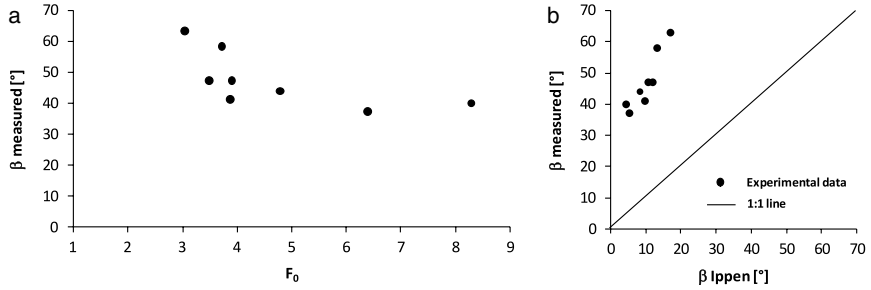

Fig. 5. Detachment angle β as a function of F_0 and comparison of the experimental values of β with theoretical values [24].

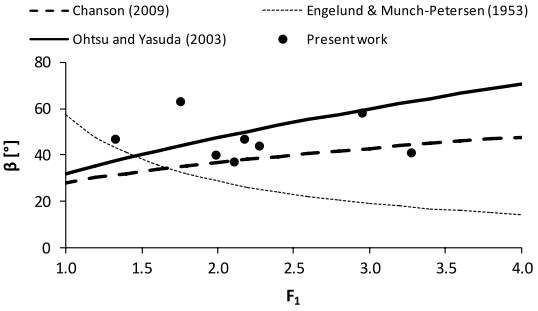

Fig. 6. Detachment angle β as a function of F_1.

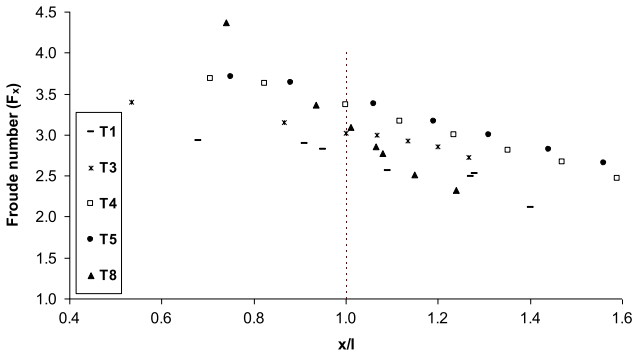

Fig. 7. Froude number measured at the channel centreline as a function of x/l.

Fig. 7 shows the variation of the local Froude number, F_x, along the channel centreline as a function of the dimensionless longitudinal distance x/l. Each value of F_x refers to a single measurement point along the channel centreline. It was calculated using the longitudinal time-averaged flow velocity and the water depth in the analyzed measurement point along the channel centreline for $x < L$. The data refer only to tests T1, T3, T4, T5 and T8, while for tests T2, T6 and T7 the data along the channel centreline were not sufficient to show a clear trend. Fig. 7 clearly shows the decrease of the Froude number as x/l increases, which is a logical and normal trend for the flow upstream of a hydraulic jump. However, attention is subsequently drawn to the rate of decrease of F_x which is obviously linked to the Froude number F_0 (see Table 1). In addition, at $x/l = 1$ (toe of the jump), it can be seen that the values of F_x range from 2.5 to 3.5, which is smaller than that of F_0 and comparable with that analyzed by other authors who assessed similar measurements.

4.2. Boundary layer thickness at the lateral sidewall

Fig. 8(a) and (b) show an example of the dimensionless longitudinal velocity U/U_i-profiles upstream and in proximity of the detachment point at different longitudinal locations x/l far from the upstream channel gate, where U is the time-averaged longitudinal velocities at the longitudinal position x and transversal position y and U_i is the mean free-stream water velocity, within the cross section at the longitudinal position x. For these purposes, data refer to tests T3 and T4.

An examination of these figures clearly shows that upstream of the detachment point, $x/l < 1$, the U/U_i-values remain quasi-constant and with an order of magnitude of 1, as the transversal position from the channel wall $y/(B/2)$ increases until the longitudinal channel centreline $y/(B/2) = 1$. This implies that in the supercritical flow zone the lateral wall boundary layer remains very close to the channel sidewall and its thickness δ is extremely small. At $x/l < 1$, the U/U_i-profiles of Fig. 8(a) and (b) give values of δ less than $0.024l$ and $0.029l$ for tests T3 and T4, respectively. These values were estimated on the basis of the position of $U/U_i = 0.99$ of the U/U_i-profiles. For both tests, close to the detachment point where $x/l \approx 1$, a significant increase of U/U_i-values can be noted from the channel sidewall up to $y/(B/2) \approx 0.20$, while they remain quasi-constant for $y/(B/2) > 0.20$.

The enlargement of the zone close to the channel sidewall where a high value of the velocity gradient $\partial U/\partial y$ is present implies an increase in the boundary layer thickness δ which becomes $0.22l$ at the detachment point for both tests T3 and T4. At the detachment point of test T4 (Fig. 8(b) at $x/l = 1$), the

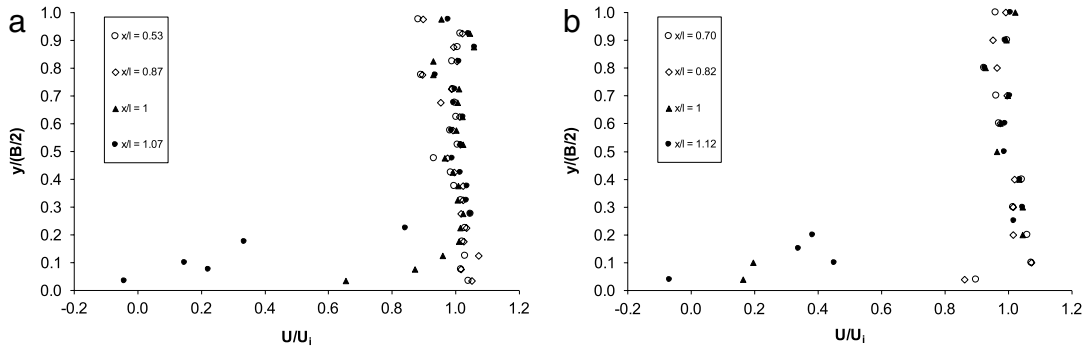

Fig. 8. Dimensionless transversal velocity U/U_i- profiles upstream and around the detachment point: (a) T3 ($F_0 = 3.72$), (b) T4 ($F_0 = 3.89$).

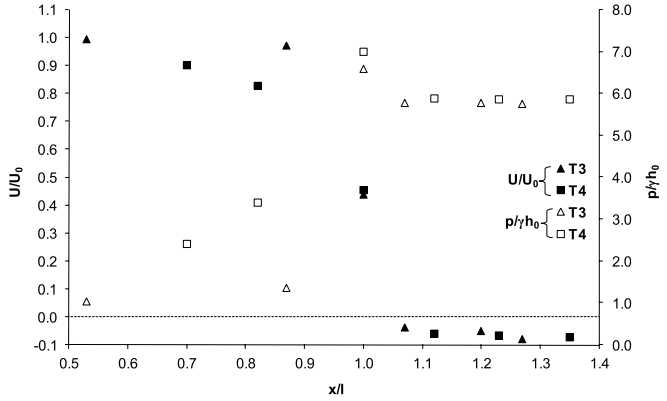

Fig. 9. Dimensionless longitudinal velocity component U/U_0 and pressure $p/\gamma h_0$ as function of x/l. Distributions along the sidewall at $y/(B/2) = 0.04$ for tests T3 and T4.

U/U_i-profile shows a point of inflection between $y/(B/2) = 0.2$ and $y/(B/2) = 0.1$ and the velocity gradient reaches a value of $\partial U/\partial y \approx 0$ at a distance less than $y/(B/2) = 0.1$ from the wall. This value confirms that the separation of the boundary layer occurs at the detachment point. At $x/l = 1.07$ and 1.12 for tests T3 and T4, respectively, the U/U_i-profiles show negative values close to the boundary wall, revealing the development of backflow patterns.

The backflow velocity profiles are due to an adverse pressure gradient. In fact, the longitudinal adverse pressure gradient near the sidewall is shown in Fig. 9 for tests T3 and T4 with the dimensionless velocity U/U_0. The pressure was determined using the measured velocity data assuming a hydrostatic pressure, neglecting the energy losses in the flow regions upstream and downstream of the detachment point and considering only the local energy loss due to the hydraulic jump (more details on the energy losses are reported below). Fig. 9 clearly shows that downstream of the detachment point ($x/l = 1$) the longitudinal velocity becomes negative due to the adverse pressure gradient.

Taking into consideration normal experimental errors and slight oscillations of the jump front (also described in literature, see for example [27,28,12,29,30], it is necessary to underline that the experimental values of l, i.e. of the distance from the channel upstream gate to the jump toe, are characterized by an accuracy of 2 cm.

4.3. Displacement thickness

Since the sidewall boundary layer thickness δ is extremely small and due to the lack of measured flow velocity data at $y/(B/2) < 0.03$, an estimate of the displacement thickness δ^* of the turbulent boundary layer was carried out using Eq. (3). For test T3, the estimated δ^* is $0.0015l$ and $0.0023l$ at $x/l = 0.53$ and 0.87, respectively, while for test T4 it is $0.0018l$ and $0.0021l$ at $x/l = 0.70$ and 0.82, respectively. It should be borne in mind that the values of δ^* for $x/l < 1$ were estimated using Eq. (3) with the experimental data of U_i at each transversal section.

Taking into account that the value of the displacement thickness varies from one-eighth to one-tenth of the boundary layer thickness δ, as mentioned previously, the use of Eq. (3) is appropriate, since δ has a magnitude order of $0.024l$ and $0.029l$ for tests T3 and T4, respectively.

Since an adequate amount of velocity data were available near the detachment point, very close to the wall and along the transversal flow direction, here δ^* was calculated using Eq. (2). It was observed that, at the detachment point, Eq. (3) strongly underestimates the values of the observed displacement thickness δ^* due to its sudden increase at this position.

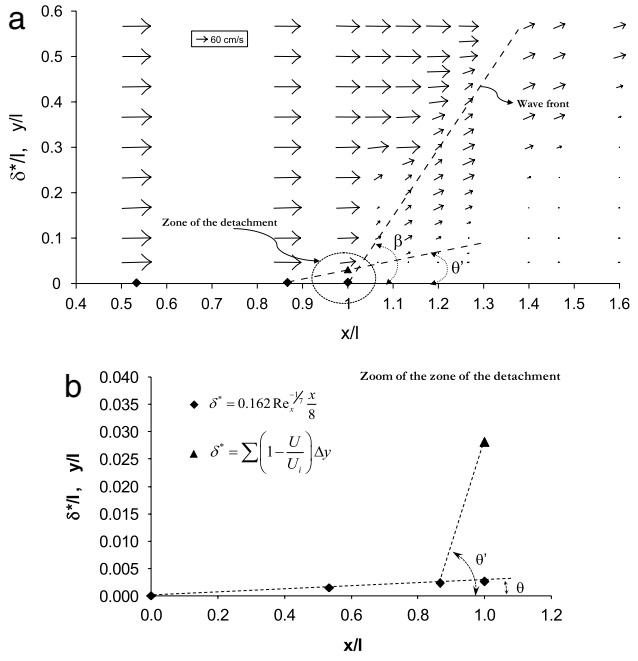

Fig. 10. Sharp increase of the displacement thickness δ^* at the detachment point ($x/l = 1$) for test T3 ($F_0 = 3.72$). (a) Flow field close to the oblique front; (b) enlargement close to the lateral channel wall.

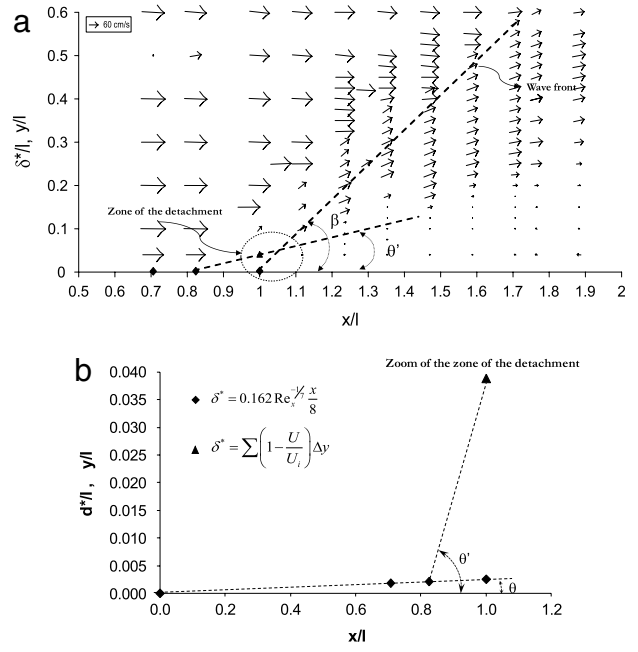

Fig. 11. Sharp increase of the displacement thickness δ^* at the detachment point ($x/l = 1$) for test T4 ($F_0 = 3.89$). (a) Flow field close to the oblique front; (b) enlargement close to the lateral channel wall.

Figs. 10(a) and (b) and 11(a) and (b) show the dimensionless displacement thickness δ^*/l for tests T3 and T4, respectively, as a function of the dimensionless distance x/l. In Figs. 10(a) 11(a), in addition to the displacement thickness, the flow velocity distribution is also plotted. Firstly, the enlarged area near the detachment point (see Figs. 10(b) and 11(b)) shows a gradual increase of δ^* with x, with the formation of a virtual lateral wall inclined at an angle of $\theta \approx 0.15°$ and 0.14° with respect to the channel sidewall, for tests T3 and T4, respectively.

Moreover, the strong increase of δ^* at the detachment point can clearly be seen, reaching a value of $0.028l$, equal to nearly

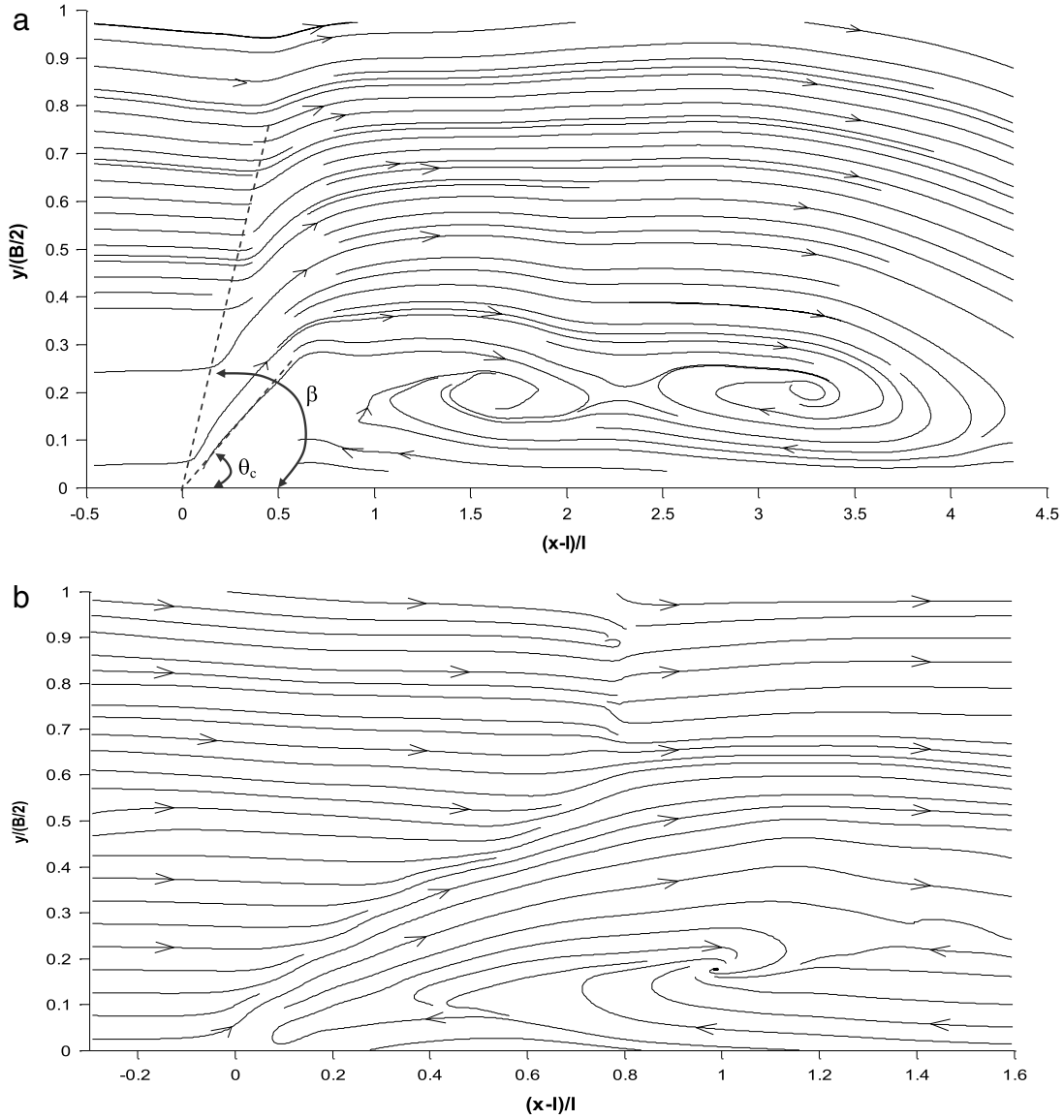

Fig. 12. Map of the flow streamlines of: (a) test T3 ($F_0 = 3.72$), (b) test T4 ($F_0 = 3.89$).

one-eighth of $\delta = 0.214l$. This value was obtained using Eq. (2) and is nearly 10 times greater than the expected value of $0.0026l$ estimated using Eq. (3). The sudden strong increase of δ^* leads to an immediate increase of the angle θ to $\theta' \approx 11°$ and 11.8° for tests T3 and T4, respectively, estimated with the value trend of δ^*. Because of the method used to calculate θ', its value is equal to, or less than, the critical value θ_c.

In particular, for test T3, where a large number of velocity measurement points were assessed, a control estimate of the critical angle, θ_c, was carried out using the map of the flow velocity streamlines shown in Fig. 12(a). Using this procedure, the value of θ_c was determined as the angle that the most inclined streamline forms with the lateral wall downstream of the oblique front of the hydraulic jump. The value of θ_c was equal to 15° which is comparable with the value of θ'.

A recirculation zone is clearly visible downstream of the detachment point. It can be noted that θ_c is smaller than the divergence angle β of the reflected wave from the sidewall [31].

4.4. General flow features

The velocity streamlines illustrated in Fig. 12(a) and (b) clearly show the flow features in the channel, for tests T3 and T4, respectively. At the supercritical region, the streamlines are almost parallel to the sidewall (at $y = 0$) and the longitudinal water velocity components dominate the transversal ones. The detachment point, i.e. the point of separation of the sidewall boundary layer, and the divergence of the shock wave front (angle β) are also notable. Downstream of the oblique wave front, a recirculating flow region develops, showing flow structures characterized by large clockwise vortices. Moreover, it can also be noted that far downstream of the lateral shock wave (indicated, as an example, by the dashed black line in the case of test T3), the streamlines again become almost parallel to the channel sidewall and then bend towards it. At the crossing of the two symmetrical lateral shock waves, in the centre of the channel, new reflected shock waves appear, resulting in a classical geometric system also observed in literature [3].

In order to understand the flow structures along the channel better and to illustrate the velocity redistribution around the shock wave front and in the recirculation flow area, Fig. 13 plots the normalized transversal U/U_o and V/U_o velocity profiles at different downstream locations x/l from the upstream channel gate for two typical tests, T3 (type E jump) and T4 (type D jump). In Fig. 13, the transversal distance y from the channel sidewall is

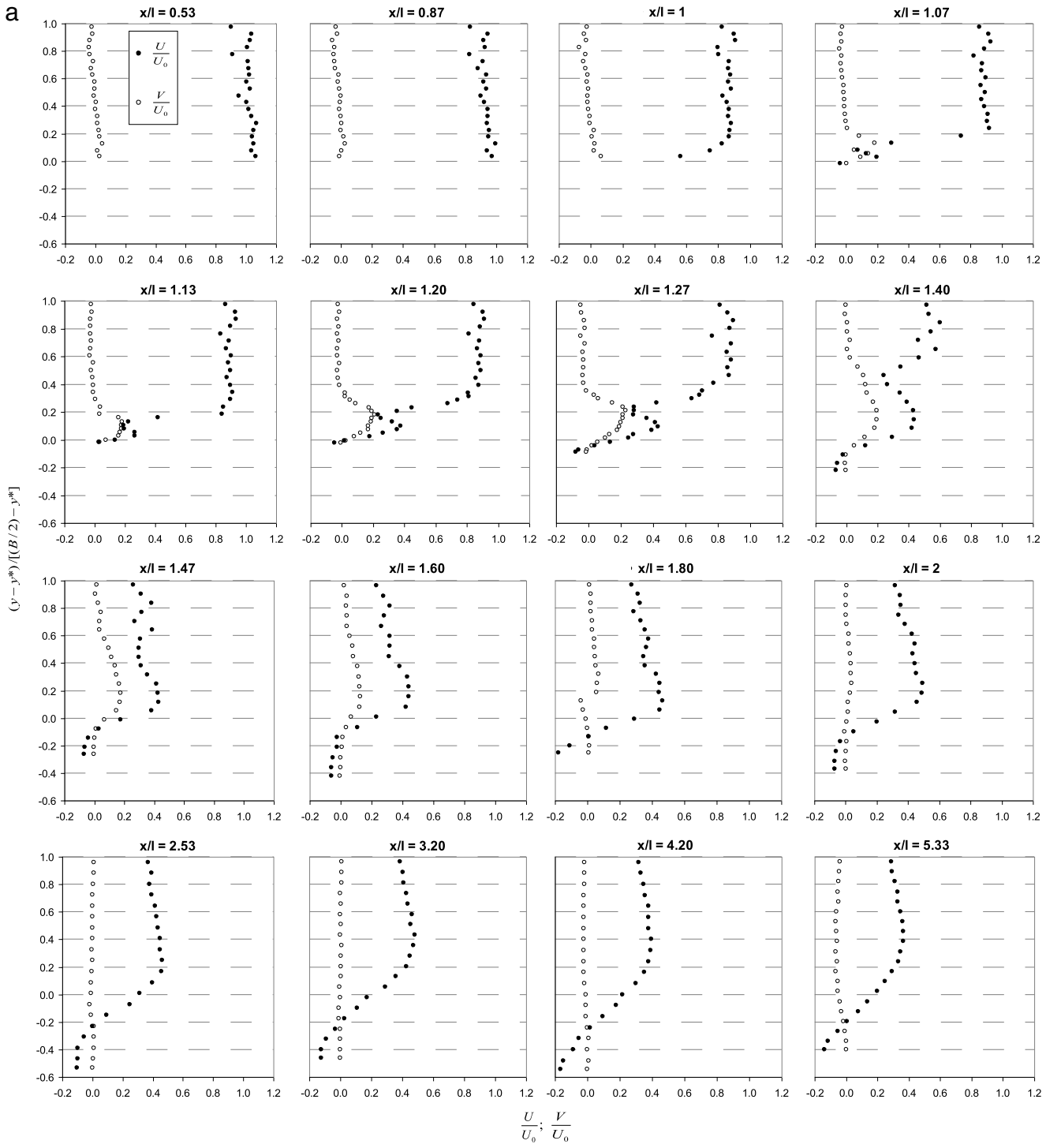

Fig. 13. Transversal profiles of U and V velocity components at different sections; (a) T3 ($L/l = 1.34, F_0 = 3.72$), (b) T4 ($L/l = 2.11, F_0 = 3.89$).

normalized as $(y - y^*)/[(B/2) - y^*]$, where y^* is the normal distance from the channel sidewall to the position of the dividing streamline Ψ, defined as $\int_0^y U dy = 0$. Fig. 13 shows different typologies of velocity profiles for both components U and V depending on the downstream location x/l. In addition, it can be noted that the flow velocity distributions for both components U and V are not significantly influenced by the jump type and show similar behaviour for both tests T3 (type E jump) and T4 (type D jump). For both tests, three classes of profiles can be identified:

(i) Upstream of the detachment point ($x < l$), the U/U_o-values present an order of magnitude of 1 along the entire channel width, while V/U_o-values are negligible.

(ii) Between the detachment point and the position of the normal front of the jump ($l \leq x \leq L$), the velocity profiles of both velocity components can be divided into two subclasses. The first is present at the upstream region of the lateral shock wave front where the velocity profiles are similar to those

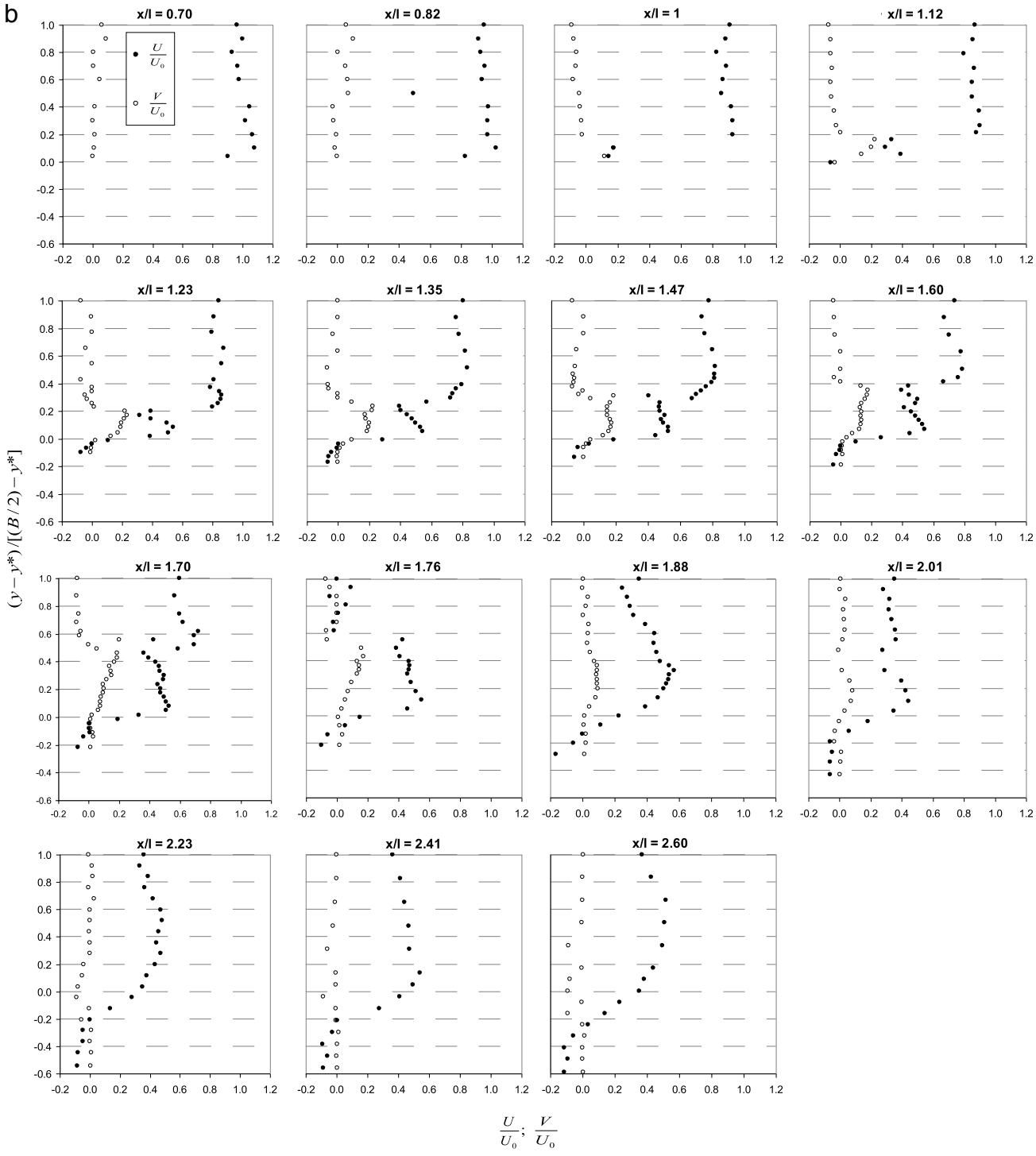

Fig. 13. (*continued*)

observed at $x < l$. The second subclass takes place at the downstream region of the lateral shock wave front where the spanwise velocity component V increases significantly, showing an absolute maximum value at the lateral shock wave front. In this region, the streamwise component U decreases dramatically to values comparable with those of V and starts to show negative values as x/l increases.

(iii) Downstream of the normal front of the jump ($x > L$), the spanwise velocity starts to decrease gradually as x/l increases, reaching small values and becoming negative at some positions. On the other hand, the streamwise velocity profiles have a similar trend, showing their absolute positive maxima at a certain distance from the longitudinal channel axis which clearly reveals the presence of vortical structures downstream of the hydraulic jump.

4.5. Measurement of flow turbulence intensities

The turbulence intensity of the flow is fundamental in understanding flow structures. In addition, it is often necessary to

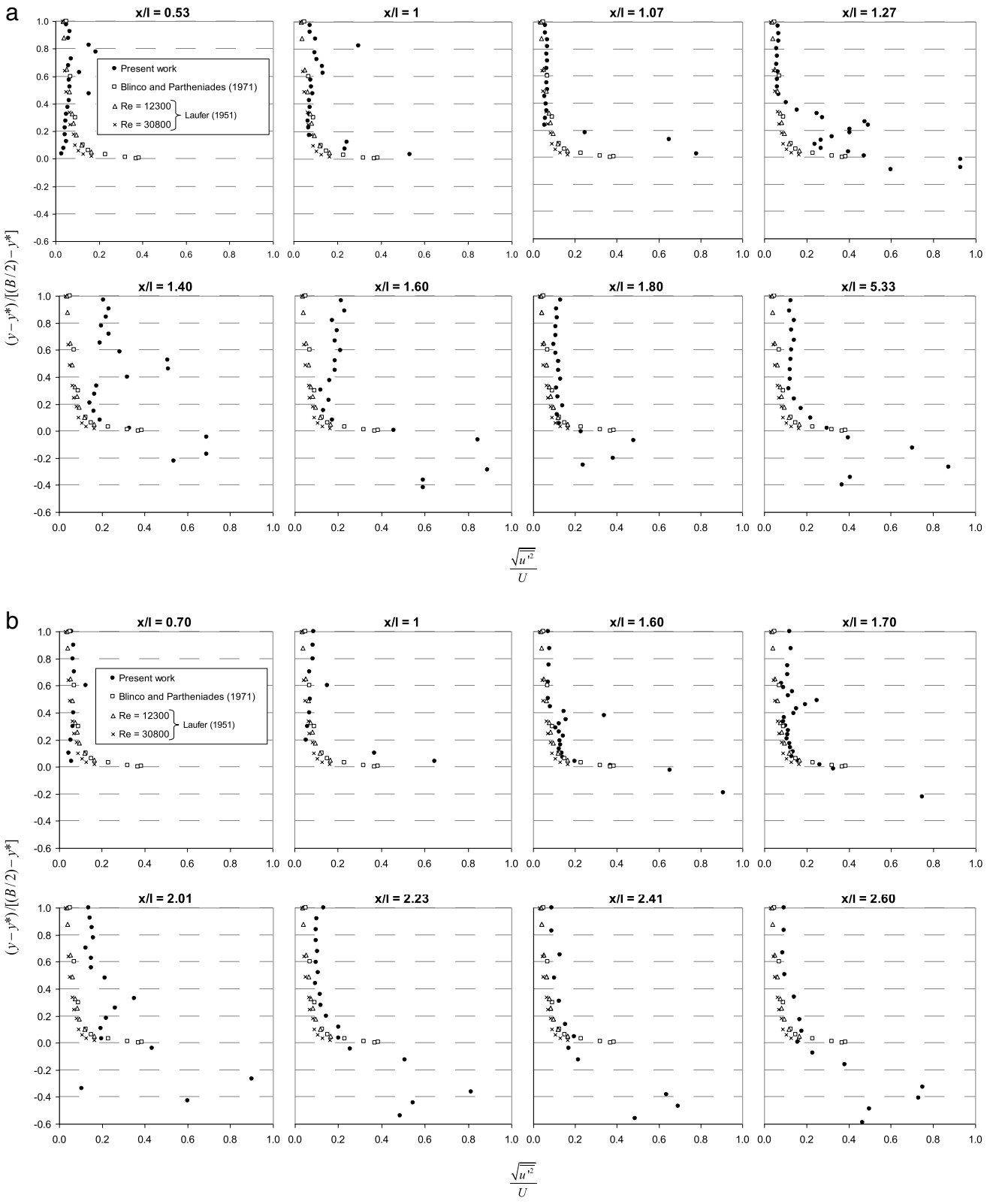

Fig. 14. Relative turbulence intensity distribution of the streamwise velocity component u; (a) T3 ($L/l = 1.34$, $F_0 = 3.72$), (b) T4 ($L/l = 2.11$, $F_0 = 3.89$).

estimate it when setting boundary conditions for computational fluid dynamic simulations. Fig. 14 illustrates the relative turbulence intensity distribution of the streamwise velocity component u. Several transversal profiles at different cross sections x/l are highlighted. The data of Fig. 14 refer to tests T3 (type E jump) and T4 (type D jump), respectively. In order to compare the measured turbulence intensities of the present study and those assessed in free surface flows over smooth boundaries, turbulence data published by Blinco and Partheniades [32] and Laufer [33] are also plotted in Fig. 14 for all the analyzed channel cross sections. The reported turbulence data of Blinco and Partheniades [32] and Laufer [33] were assessed in two-dimensional turbulent smooth

channel flows and their velocity measurement systems were a hot-film anemometer and a hot-wire anemometer, respectively. As seen before, the transversal distance y from the channel sidewall is normalized as $(y - y^*)/[(B/2) - y^*]$ in order to show all the transversal profiles, including the flow recirculation region. In fact, logically the data of Blinco and Partheniades [32] and Laufer [33] are comparable with ours only outside the recirculation flow region (where the flow velocity distributions are similar to those in two-dimensional turbulent channel flows), starting from the separated boundary layer ($\Psi = 0$). Herein, it should be also borne in mind that in the backflow region, where U shows negative values, the r.m.s. of u velocity component is dimensionlessed with the absolute value of the time-averaged longitudinal velocity component U.

The profiles in Fig. 14(a) clearly show that in the supercritical flow region, upstream of the normal shock wave front ($x \leq L$) of test T3 (type E jump), with x/l from 0.53 to 1.27, the turbulence intensity has the same order of magnitude and trend of those presented by Blinco and Partheniades [32] and Laufer [33].

As shown in Fig. 14(b), in the region from $x/l = 0.70$ to 1.60 of test T4 (type D jump), the turbulence intensity profiles are similar to those obtained in test T3 and thus they show order of magnitudes comparable to those obtained by Blinco and Partheniades [32] and Laufer [33]. In test T4 from $x/l = 1.70$ to 2.01, the magnitudes of the turbulence intensity increase compared to the values obtained by the referred authors. This implies that a major flow redistribution occurs within this region, leading to a large energy dissipation. Montes and Chanson [34] experimentally observed that the most of the energy dissipation along the centreline takes place between the beginning of the lateral shock waves and the first crest of the undular jump.

Downstream of the shock wave front and from the detachment point ($x/l = 1$) up to the normal front of the jump ($x < L$), precisely at $x/l = 1.27$ and $x/l = 2.01$ for tests T3 and T4, respectively (see Fig. 14), the turbulence intensity increases strongly, reaching values also greater than 0.6, which are surely higher than the value of about 0.1 obtained by Blinco and Partheniades [32] and Laufer [33].

Moreover, it can be clearly noted that the large magnitude of the turbulence intensity (peak of the profiles), outside the recirculation zone (i.e. for $(y-y^*)/[(B/2)-y^*] > 0$), take place along the shock wave front, leading to a significant increase of the turbulent kinetic energy. Most of the flow energy is then dissipated along the shock wave front.

From $x/l = 1.40$ to 1.60 and $x/l = 2.01$ to 2.23 for tests T3 and T4, respectively, the turbulence intensity also shows large values around the channel axis. The increase of turbulence intensity at these positions is a result of the high flow perturbation due to the normal jump front. Further downstream, from $x/l = 1.80$ to $x/l = 5.33$ and $x/l = 2.41$ to 2.60 for tests T3 and T4, respectively, the turbulence intensity profiles show the same trend proposed by Blinco and Partheniades [32] and Laufer [33], even if the magnitude of the present results are approximately two times greater than those of the cited authors. In the flow recirculation region (i.e. for $(y - y^*)/[(B/2) - y^*] < 0$), the turbulence intensities reach large values. This happens at the position where the time-averaged streamwise velocity U is very low, as shown in Fig. 13. Generally it can be noted that the turbulence intensities in the recirculation zone are always greater than 0.2.

Fig. 15 illustrates the relative turbulence intensity profiles for both the streamwise u and spanwise v velocity components in tests T3 and T4. The main aim of this figure is to highlight the importance of the v-component on the flow structures. Here, the r.m.s. of the v-fluctuation is normalized by the local time-averaged streamwise component U. It can be clearly noted that upstream of the shock wave front ($x \leq l$) in the supercritical flow region, as shown by the profiles from $x/l = 0.53$ to 1.27 and $x/l = 0.70$ to 2.01 for tests T3 and T4, the r.m.s. of v-velocities are small compared to the r.m.s. of the u-fluctuation, mainly because the flow essentially develops along the streamwise direction in the supercritical region. Downstream of the shock wave, in the region $l \leq x \leq L$, the relative turbulence intensity of the v-component increases considerably, showing the same order of magnitude as the u-component, even if it remains smaller. The peaks of the turbulence profiles, for both tests T3 and T4, take place along the shock wave front.

Near the jump front from $x/l = 1.40$ to 1.60 and $x/l = 2.01$ for tests T3 and T4, respectively, the relative turbulence intensity of the v-component increases significantly compared to the supercritical region but always remains smaller than that of the u-component. Outside the flow recirculation region, starting from $x/l = 1.80$ to 5.33 and $x/l = 2.23$ to 2.60 for tests T3 and T4, respectively, the turbulence intensity of the v-component reaches almost the same order of magnitude as the u-component and the data of both intensities appear to merge into a single profile. Inside the flow recirculation region, the v-turbulence intensities show a trend similar to that of the u-turbulence profiles, but their magnitude is smaller, especially in the region near the channel sidewalls.

4.6. Analogy between supersonic flow separation and supercritical free surface flow

Fig. 16 shows a plot of our experimental data for Eq. (5) in which the total skin friction coefficient C_f is evaluated by using Eqs. (6)–(9) in correspondence with the toe of the jumps. It can be noted that even if C_f is evaluated by using different expressions, the data fit quite well into a single, if rather narrow region, confirming the validity of Eq. (5). This implies that an analogy of the supersonic flow separation with the supercritical free surface flow of the present study is reasonably well validated. Therefore, the behaviour of a supercritical flow during separation can be interpreted with the free interaction theory.

4.7. Energy loss and drag effect due to lateral shock waves

Using a large set of experimental data, Montes and Chanson [34] evaluated energy dissipation at the channel centreline of undular hydraulic jumps. In particular they highlight that most of the energy dissipation along the channel centreline takes place between the start of the lateral shock waves and the first crest. Furthermore, they showed that the theoretical energy loss ΔE per unit weight for one-dimensional hydraulic jump in the following equation.

$$\frac{\Delta E}{k} = \frac{\left(\sqrt{1+8\,F_1^2}-3\right)^3}{16\,F_1^{2/3}\left(\sqrt{1+8\,F_1^2}-1\right)} \tag{16}$$

underestimates total energy dissipation. In Eq. (16) F_1 is evaluated at the centreline and at the toe of the jump ($x = l$). Furthermore, they proposed an equation for additional energy dissipation due to shock wave drag deriving from an analogy with the transonic drag found in aerodynamics thus

$$\frac{\Delta E_{SW}}{k} = C\frac{U_1^2}{2gkh_1}\left(\frac{B}{2tg\,\beta}\right)(F_1-1)^4 \tag{17}$$

where ΔE_{SW} is the additional energy loss due to the shock wave and C is the equation parameter.

In the present paper, the total energy loss along a streamline at the channel centreline was evaluated between the jump toe and a point immediately downward of the first wave crest of

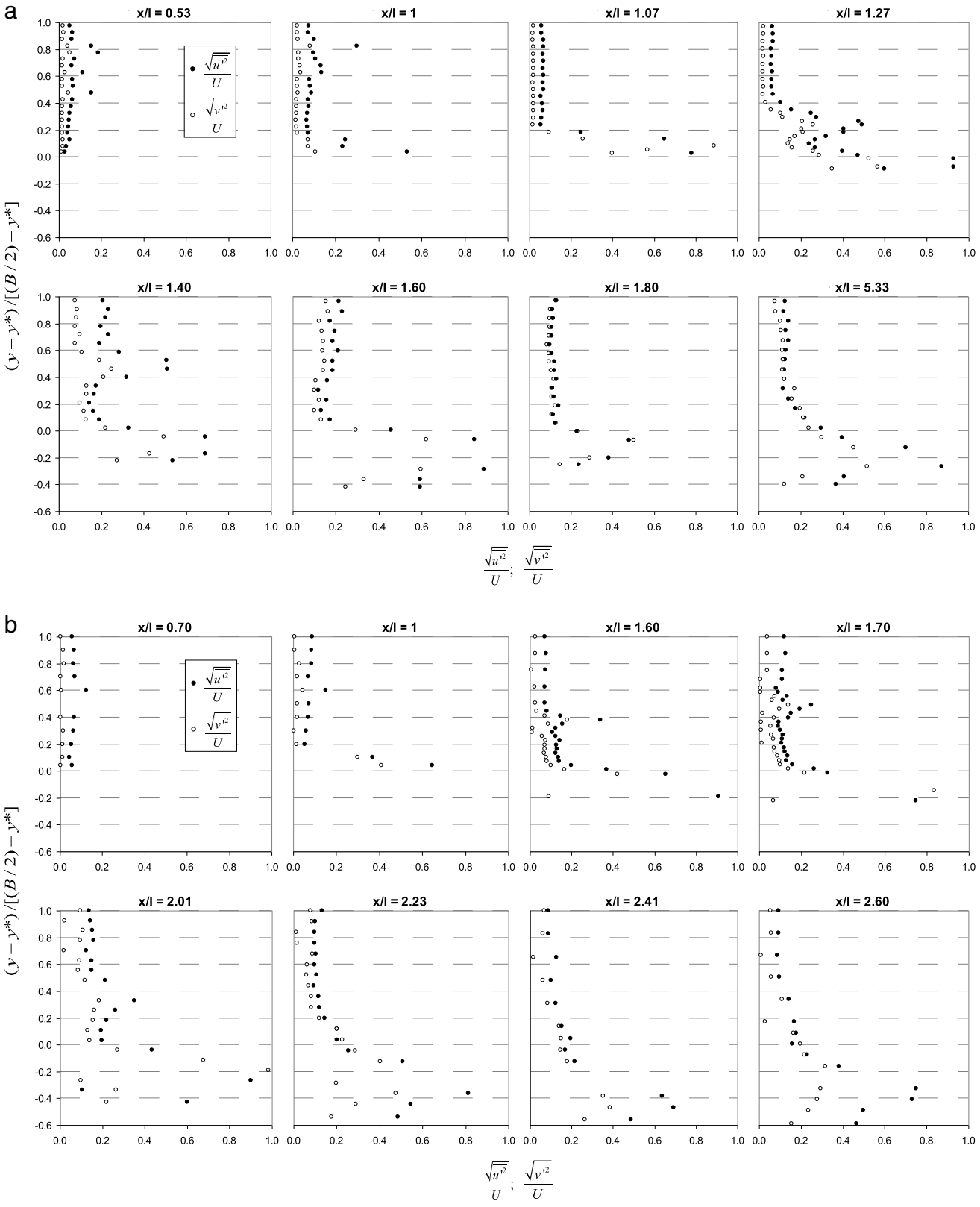

Fig. 15. Comparison between the spanwise and streamwise turbulence intensities; (a) T3 ($L/l = 1.34, F_0 = 3.72$), (b) T4 ($L/l = 2.11, F_0 = 3.89$).

the normal front of the hydraulic jump applying the Bernoulli equation. Assuming that the total energy loss is equal to the sum of the theoretical energy loss ΔE of Eq. (16) and the additional energy loss due to the shock wave ΔE_{SW} of Eq. (17), the values of coefficient C in the tests of the present study were evaluated. The result is shown in Fig. 17.

From the experimental data of the present study it is possible to see that C can be evaluated as a function of F_1 with the following

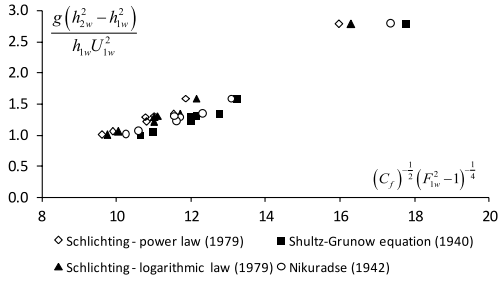

Fig. 16. Plot of the experimental data for relationship (5) with which C_f is evaluated from different expressions.

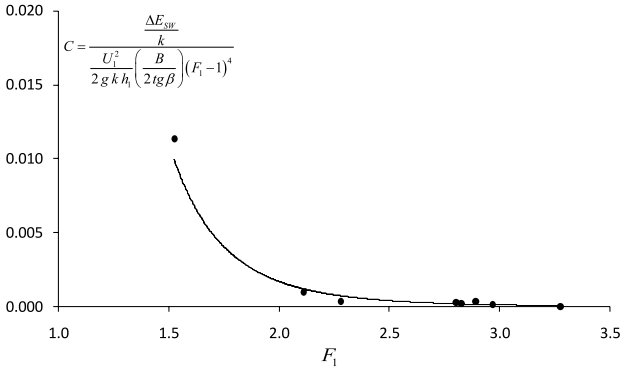

Fig. 17. Parameter C as a function of the Froude number at the jump toe.

equation

$$C = 0.233F_1^{-6.90} \qquad R^2 = 0.90. \tag{18}$$

Fig. 18 shows the dimensionless total energy losses of our experimental data at the jump toe in the channel centreline as a function of the Froude numbers. Fig. 18 also shows the experimental data of Montes and Chanson [34] in addition to the total energy losses obtained by the sum of Eqs. (16) and (17), in which coefficient C is calculated from Eq. (18).

The results highlight that also in the present study energy losses are higher than those predicted by the theoretical equation (16), with the differences almost certainly attributable to the additional drag due to the lateral front of the shock wave, as suggested by Montes and Chanson [34]. Furthermore, Fig. 18 shows that the total energy loss given by the sum of Eqs. (16) and (17) is generally in good agreement with the experimental results obtained by Montes and Chanson [34].

5. Conclusions

In the present study the fundamental importance of the interaction between boundary layer and shock waves was highlighted.

Firstly, the authors pointed out the increase of the detachment angle β with the inflow Froude number F_0, in agreement with the classical theory of oblique shock waves outlined by Ippen [24]. On the other hand, considering the Froude number F_1 at the jump toe, the detachment angle β increases with F_1. The results show that both numbers are important in jump developments, the first affecting the longitudinal position of the detachment point and the second the jump type.

Upstream of the toe of the oblique shock waves, the displacement thickness δ^* shows a slight yet gradual increase, forming a virtual lateral wall inclined at an angle θ with respect to the channel sidewall. At the detachment point, δ^* experiences a sudden rise, with an immediate increase in angle θ to a critical value θ_c. Moreover, it was observed that at the detachment point and in the flow region close to the channel sidewall a sudden adverse pressure gradient occurs. Under these conditions a separation of the boundary layer takes place and there is a detachment of the lateral shock wave.

An analysis of the distribution of flow velocity components and their streamlines confirms a symmetrical flow reflection towards the channel sidewalls downstream of the intersection point of the two lateral shock waves that are responsible for the trapezoidal shape of the jump. It was also observed that the first intersection of the shock waves is always near the top of the first wave crest, which is in good agreement with the results of Chanson and Montes [3].

An analysis of the flow velocity distribution and the background turbulence intensity of both velocity components u and v shows that flow structures can be divided into three classes depending on the type of velocity profiles as well as the flow recirculation area. In the region where the flow is supercritical, the current is mono-dimensional in the streamwise direction. In this region, the relative turbulence intensity of the u-component is in good agreement with the data of Blinco and Partheniades [32] and Laufer [33], who assessed measurements in two-dimensional turbulent smooth channel flows.

Outside the supercritical region, it was observed that the flow undergoes a large perturbation downstream of the shock wave front at $l \leq x \leq L$ where both a reduction of the streamwise time-averaged U velocity component and an increase of the spanwise time-averaged V velocity component occur. This perturbation is due to the separation of the turbulent boundary layer, with a significant increase in the turbulence intensities of both the u and v velocity components.

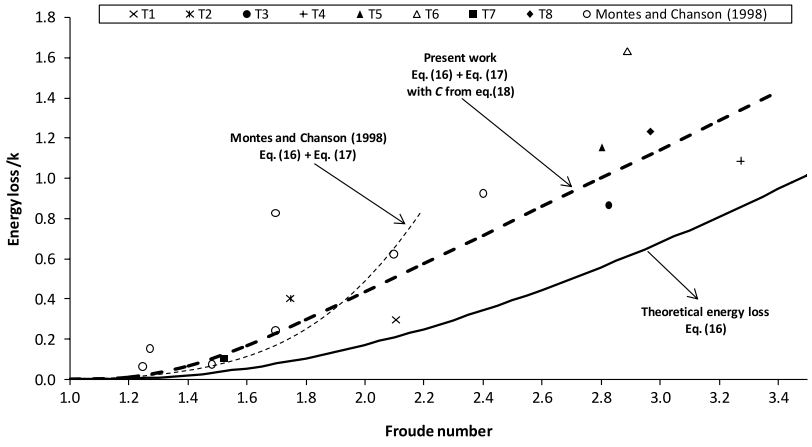

Fig. 18. Energy loss due to the jump in the presence of a lateral shock wave as a function of the Froude number at the jump toe.

At the channel axis, close to the hydraulic jump front, the turbulence intensities of both velocity components also show large values. Just downstream of the hydraulic jump front, the turbulence intensity of the v-component is always smaller than that of the u-component even if they show the same trend profiles.

Starting from $x > L$, outside the flow recirculation region, the turbulence intensity of the v-component reaches almost the same values as the u-component. Here the values of both intensities appear almost to merge into a single profile. In addition, the u-turbulence intensity profiles of the present study show the same trend as that of Blinco and Partheniades [32] and Laufer [33] but with approximately double the magnitude.

In the flow recirculation region the profiles of the turbulence intensities show an asymptotic trend to larger values (which are greater than a magnitude of 1) for both velocity components.

Furthermore, it was argued that the supersonic flow separation theory can be used in the case of the supercritical free surface flow analyzed in the present study and that the behaviour of a supercritical flow during separation can be interpreted with the free interaction theory.

The authors also investigated additional energy losses due to shock wave formation. It was observed that the equation proposed by Montes and Chanson [34] can be adopted to calculate total energy losses due to shock wave formation, assuming a variability in parameter C with the Froude number using the experimental law presented in this paper.

References

[1] V.T. Chow, Open Channel Hydraulics, McGraw-Hill Book Company, New York, 1959.
[2] I. Ohtsu, Y. Yasuda, H. Gotoh, Flow conditions of undular hydraulic jumps in horizontal rectangular channels, J. Hydrau. Eng. 129 (12) (2003) 948–955.
[3] H. Chanson, J.S. Montes, Characteristics of undular hydraulic jump: experimental apparatus and flow patterns, J. Hydrau. Eng. 121 (2) (1995) 129–144.
[4] M. Ben Meftah, F. De Serio, M. Mossa, A. Pollio, Undular jump formation in very large channel, in: Proceedings of IDRA 2006, Italian Conference of Hydraulics and Hydraulic Construction, Roma, 10–15 September, 2006.
[5] M. Ben Meftah, F. De Serio, M. Mossa, A. Pollio, Analysis of the velocity field in a large rectangular channel with lateral shock wave, Environ. Fluid Mech. 7 (6) (2007) 519–536.
[6] M. Ben Meftah, F. De Serio, M. Mossa, A. Pollio, Experimental study of recirculating flows generated by lateral shock waves in very large channels, Environ. Fluid Mech. 8 (6) (2008) 215–238.
[7] R. Reinauer, W.H. Hager, Non-breaking undular hydraulic jumps, J. Hydrau. Res. 33 (5) (1995) 1–16.
[8] H. Chanson, Non-breaking undular hydraulic jump — discussion, J. Hydrau.s Res., IAHR 34 (2) (1996) 279–287.
[9] I. Ohtsu, Y. Yasuda, H. Gotoh, Characteristics of undular jump in rectangular channels, in: Proc., XXVI Int. Association for Hydraulic Research Congress, London, 1C14, 1995, pp. 450–455.
[10] I. Ohtsu, Y. Yasuda, H. Gotoh, Hydraulic condition for undular-jump formations, J. Hydrau. Res. 39 (2) (2001) 203–209.
[11] M. Mossa, U. Tolve, Flow visualization in bubbly two-phase hydraulic jump, Trans. ASME 120 (1) (1998).
[12] M. Mossa, On the oscillating characteristics of hydraulic jump, J. Hydrau. Res. 37 (4) (1999) 541–558.
[13] J.S. Montes, A Study of the undular jump profile, in: Proc. 9th Australasian Fluid Mechanics Conference AFMC, Auckland, New Zealand, 1986, pp. 148–151.
[14] R. Reinauer, W.H. Hager, Shock wave in air-water flows, J. Multiphase Flow 22 (6) (1996) 1255–1263.
[15] D. Arnal, J. Délery, Laminar-turbulent transition and shock wave/boundary layer interction, Paper presented at the RTO AVT Lecture Series on Critical Technologies for Hypersonic Vehicle Development, held at the von Kàrmàn Institute, Rhode-St-Genèse, Belgium, 10–14 May, 2004, and published in RTO-EN-AVT-116, 2004.
[16] H. Schlichting, Boundary Layer Theory, 7th ed., McGraw-Hill, New York, 1979.
[17] D.R. Chapman, D.M. Kuehn, H.K. Larson, Investigation of separated flows in supersonic and subsonic streams with emphasis on the effect of transition, NACA Tech. Note 3867, 1957, pp. 419–460.
[18] M.J. Lighthill, On boundary layers and upstream influence. II. Supersonic flows without separation, Proc. R. Soc. Lond. A 217 (1953) 478–507.
[19] K.W. Cassel, A.I. Ruban, J.D.A. Walker, An instability in supersonic boundary layer flow over a compression ramp, J. Fluid Mech. 300 (1995) 265–285.
[20] H. Chanson, The Hydraulic Open Channel Flow: An Introduction, Edward Arnold, London, 1999.
[21] J.A. Liggett, Fluid Mechanics, McGraw-Hill, New York, USA, 1994.
[22] F. Shultz-Grunow, Neues Widerstand fur glatte Platten, Luftfahrtfforschung 17 (1940) 239–246 (in German).
[23] J. Nikuradse, Turbulente reibungsschichten and der platte, ZWB. R. Oldenbourg, Munchen, Berlin, 1942 (in German).
[24] A.T. Ippen, Mechanics of supercritical flow, Trans. ASCE 116 (1951) 268–295.
[25] H. Chanson, Current knowledge in hydraulic jumps and related phenomena. A survey of experimental results, Eur. J. Mech. B Fluids 28 (2009) 191–210.
[26] F. Engelund, J. Munch-Petersen, Steady flow in contracted and expanded rectangular channels, Some considerations concerning the shape of the water surface, Jl La Houille Blanche, Aug./Sept., 1953, pp. 464–474.
[27] G. Nebbia, Su taluni fenomeni alternativi in correnti libere, L'Energia Elettrica XIX (1942) 1–10 (in Italian).
[28] D. Long, N. Rajaratnam, P.M. Steffler, P.R. Smy, Structure of flow in hydraulic jumps, J. Hydrau. Res., IAHR 29 (2) (1991) 207–218.
[29] H. Chanson, T. Brattberg, Experimental study of the air-water shear flow in a hydraulic jump, Internat. J. Multiphase Flow 26 (2000) 583–607.
[30] S. Kucukali, H. Chanson, Turbulence measurements in the bubbly flow region of hydraulic jumps, Exper. Thermal Fluid Sci. 32 (2008) 41–53.
[31] P.A. Carling, Flow-separation berms downstream of a hydraulic jump in a bedrock channel, Geomorphology 11 (1995) 245–253.
[32] P.H. Blinco, E. Partheniades, Turbulence characteristics in free surface flows over smooth and rough boundaries, J. Hydrau. Res. 9 (1) (1971) 43–71.
[33] J. Laufer, Investigation of turbulent flow in a two-dimensional channel, NACA, Report 1053, 1951, pp. 1247–1266.
[34] J.S. Montes, H. Chanson, Characteristics of undular hydraulic jump: experiments and analysis, J. Hydrau. Eng. 124 (2) (1998).